



# CHORUS

This is the accepted manuscript made available via CHORUS. The article has been published as:

## Edge States and Topological Pumping in Spatially Modulated Elastic Lattices

Matheus I. N. Rosa, Raj Kumar Pal, José R. F. Arruda, and Massimo Ruzzene

Phys. Rev. Lett. **123**, 034301 — Published 17 July 2019

DOI: [10.1103/PhysRevLett.123.034301](https://doi.org/10.1103/PhysRevLett.123.034301)

# Edge states and topological pumping in spatially modulated elastic lattices

Matheus I. N. Rosa<sup>a</sup>, Raj Kumar Pal<sup>b</sup>, José R.F. Arruda<sup>c</sup> and Massimo Ruzzene<sup>a,b</sup>

<sup>a</sup> *School of Mechanical Engineering, Georgia Institute of Technology, Atlanta GA 30332*

<sup>b</sup> *School of Aerospace Engineering, Georgia Institute of Technology, Atlanta GA 30332 and*

<sup>c</sup> *School of Mechanical Engineering, State University of Campinas (UNICAMP), Campinas, SP, Brasil*

Spatial stiffness modulations defined by the sampling of a two-dimensional surface provide one-dimensional elastic lattices with topological properties that are usually attributed to two-dimensional crystals. The cyclic modulation of the stiffness defines a family of lattices whose Bloch eigenmodes accumulate a phase quantified by integer valued Chern numbers. Non-trivial gaps are spanned by edge modes in finite lattices whose location is determined by the phase of the stiffness modulation. These observations drive the implementation of a topological pump in the form of an array of continuous elastic beams coupled through a distributed stiffness. Adiabatic stiffness modulations along the beams' length lead to the transition of localized states from one boundary, to the bulk and, finally, to the opposite boundary. The first demonstration of topological pumping in a continuous elastic system opens new avenues for its implementation on elastic substrates supporting surface acoustic waves, or to structural components designed to steer waves or isolate vibrations.

The investigation of topologically protected modes for robust waveguiding along boundaries or interfaces has attracted significant interest across different physical realms, including quantum [1], electromagnetic [2], acoustic [3, 4] and elastic [5] media. In mechanics, topologically protected modes have been successfully observed by establishing Quantum hall effect (QHE) and quantum spin Hall effect (QSHE) analogues through time-reversal symmetry [6–11] and spatial symmetry [5, 12–16] breaking.

Recently, topological waveguiding has been pursued by accessing higher dimensional topological effects in lower dimensional systems [17, 18]. This approach has been exploited to induce adiabatic pumping of waves in one-dimensional (1D) quasi-periodic photonic waveguides [19, 20], and to implement a four-dimensional (4D) quantum Hall system through two-dimensional (2D) periodic arrays [21]. Also, localized modes in a chain of mechanical spinners arranged in patterns obtained by projections from manifolds have been studied in [22]. In this letter, we investigate a family of 1D elastic lattices where nearest-neighbor interactions are defined by the sampling of a 2D surface, in a configuration inspired by the Aubry-André-Haper model [23, 24]. In line with previous work in photonics and quantum mechanics [19, 25], we show that the non-trivial topological properties of the lattice family are related to the existence of edge states for individual, finite 1D lattices. We then consider an array of continuous beams elastically coupled by a distributed stiffness modulated along the beams' length. Such a system, although continuous in nature, is gov-

erned by an eigenvalue problem of the same form as the discrete lattice family, and, therefore, has similar topological properties. This array supports of a topological pump, whereby the edge modes propagate along the beams' length, and undergo an adiabatic edge-to-edge transition produced by varying the phase of the coupling stiffness modulation. This first demonstration of a topological pump in a continuous elastic system opens new avenues for the physical implementation of topology-based wave guiding in mechanics, which has potential technological relevance for guiding of surface, guided and bulk waves in acoustic devices, ultrasonic imaging and non-destructive evaluation.

We consider a 1D lattice (Fig. 1(a)) of equal masses  $m$ , equally spaced by a unit distance, and connected by springs whose constant  $k_n$  is defined by sampling the 2D surface  $\mathcal{S}(x, \phi) = \cos(2\pi\tau x + \phi)$  at  $x_n = n$  (Fig. 1(b)). Its topological properties are defined by specific choices and variations of  $\{\tau, \phi\}$ , and lead to localized states at the boundaries of finite lattices, for both rational and irrational  $\tau$  values [19, 25]. Herein, we consider  $\tau = p/q$ , where integers  $p$  and  $q$  are co-prime defining a periodic lattice with  $q$  masses per unit cell. Accordingly, the spring constant  $k_n$  is defined as

$$k_n = k_0 \left[ 1 + \alpha \cos \left( 2\pi n \frac{p}{q} + \phi \right) \right]. \quad (1)$$

A family of lattices is associated with different values of  $\phi$ , which is regarded as an additional dimension remnant of the projection from  $S(x, \phi)$ . The cross-sections (blue lines) in Fig. 1(b) show the spring constant variation along the lattice for  $\tau = p/q = 1/3$

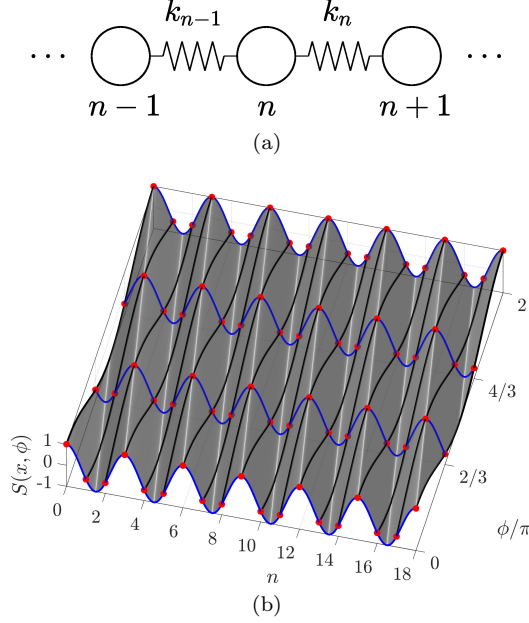


FIG. 1. (a) Spatially modulated 1D lattices with modulated stiffness  $k_n = k_0[1 + \alpha \cos(2\pi n p/q + \phi)]$ . (b) Surface  $S(x, \phi) = \cos(2\pi r x + \phi)$  generating the stiffness constants by sampling at  $x_n = n$ . (Black lines: stiffness variation with  $\phi$  at a lattice site, blue lines: cross sections at  $\phi_r = (2\pi r/3)$  ( $r \in [0, 3]$ ) with the red dots showing the sampled stiffness values.

and  $\phi_r = (2\pi r/3)$  ( $r \in [0, 3]$ ), which illustrates that  $k_n(\phi + 2\pi/q) = k_{n+s}(\phi)$ , where  $s$  obeys the algebraic congruence relation

$$ps \equiv 1 \pmod{q}. \quad (2)$$

Equation (2) has two solutions in the range  $|s| < q$  [26], which define two shifts of stiffness in opposite directions along the lattice. For  $p/q = 1/3$  (Fig. 1(b)), the solutions  $s_{1,2} = \{1, -2\}$  correspond respectively to a shift of one position to the left and of two positions to the right.

The effect of these stiffness shifts on the dispersion topology is investigated by expressing the equation for longitudinal motion of mass  $n$  at frequency  $\omega$  as

$$m\omega^2 u_n = (k_n + k_{n-1})u_n - k_n u_{n+1} - k_{n-1} u_{n-1}. \quad (3)$$

Imposing Bloch periodicity conditions  $u_{n+q} = e^{i\mu} u_n$ , where  $\mu$  is the non-dimensional wavenumber, leads to the eigenvalue problem

$$\mathbf{K}(\mu, \phi) \mathbf{u} = \Omega^2 \mathbf{u}, \quad (4)$$

where  $\mathbf{K}(\mu, \phi)$  is a stiffness matrix and  $\Omega = \omega/\omega_0$  is a non-dimensional frequency, with  $\omega_0 = \sqrt{k_0/m}$ .

Solution for  $\mu \in [0, 2\pi]$  gives a set of eigenvalues and eigenvectors that are defined by  $\phi$ , whose smooth cyclic variation, *i.e.*  $\phi \rightarrow \phi + 2\pi$ , leads to a phase accumulation (see details in the Supplementary Materials (SM) [27])

$$\mathbf{u}(\mu, \phi + 2\pi) = e^{is\mu} \mathbf{u}(\mu, \phi). \quad (5)$$

This phase accumulation is indicative of the non-trivial topology of the Bloch eigenmodes  $\mathbf{u}(\mu, \phi)$  and is quantified by the Chern number of this vector field in the  $(\mu, \phi) \in \mathbb{T}^2 = [0, 2\pi] \times [0, 2\pi]$  space [7, 28]:

$$C = \frac{1}{2\pi i} \int_{\mathcal{D}} \nabla \times \mathbf{A} d\mathcal{D}, \quad (6)$$

where  $\mathcal{D} = \mathbb{T}^2$ ,  $\nabla = (\partial/\partial\mu)\mathbf{e}_\mu + (\partial/\partial\phi)\mathbf{e}_\phi$  and  $\mathbf{A} = \mathbf{u}^* \cdot \nabla \mathbf{u}$ , with  $()^*$  denoting a complex conjugate. Analytical evaluation of the Chern number according to the procedure detailed in the SM [27] gives  $C = s$ , where  $s$  is one of the solutions of Eqn. (2). Among the two solutions, the Chern number is numerically evaluated using the procedure described in [29], which yields the results displayed in Fig. 2(a). A label for gap  $r$  is given by the algebraic sum of the Chern numbers of the bands below it, *i.e.*  $C_g^{(r)} = \sum_{n=1}^r C_n$  [30]. This gives  $C_g^{(1)} = 1$  and  $C_g^{(2)} = -1$  for the lattice considered herein (Fig. 2(a)). Non-zero gap labels signal the presence of topological edge modes spanning the bandgaps as the phase parameter  $\phi$  varies [25, 31]. This is illustrated for a free-free lattice with  $N = 60$  masses,  $p/q = 1/3$ ,  $N/q = 20$  unit cells, and  $\alpha = 0.6$ . Figure 2(b) shows the eigenfrequencies (black lines), superimposed to the bulk bands depicted by the shaded gray areas. The presence of two additional modes (red lines) spanning the bandgaps is a notable feature of the finite system spectrum, where solid and dashed lines indicate modes localized at the right and left boundary, respectively. The localized states of the finite system change their localization edge as their branches touch the boundaries of the corresponding gaps. An example of such transition for the edge mode in the second gap is shown in Fig. 2(c). The transitions are characterized by the gap label, which measures singularities (zero components) of the Bloch eigenvectors along the branch defining the lower boundary of the gap [31]. Its absolute value  $|C_g|$  equals the number of times the left (or right) edge state traverses the gap for  $\phi \in [0, 2\pi]$ . In Fig. 2, both gap labels are  $|C_g| = 1$ , which indicates that the associated edge states traverse the gap once.

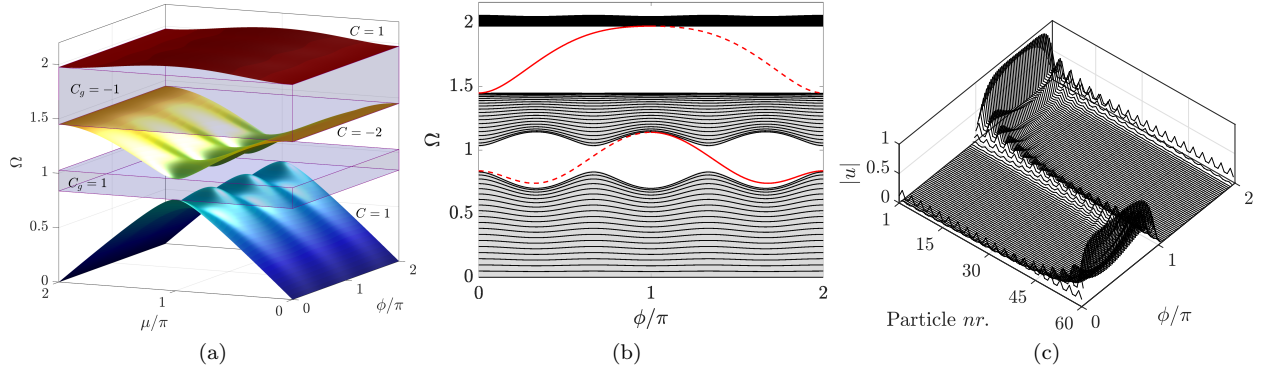


FIG. 2. Dispersion properties for  $p/q = 1/3$ ,  $\alpha = 0.6$  lattice. (a) Dispersion surfaces as a function of  $\mu$  and  $\phi$  showing 3 bulk bands and two bandgaps. Corresponding Chern numbers and gap labels are added for convenience. (b) Natural frequencies of a commensurate finite chain of 60 masses and their variation in terms of  $\phi$  (black lines) superimposed to the bulk bands (shaded gray regions), where edge modes (red lines) span the gaps. (c) Magnitude of the topological mode in the second gap and its the transition from right to left localization resulting from the variation of  $\phi$ .

Furthermore, the gap label sign defines the direction of the transition:  $C_g > 0$  defines a right-to-left transition for increasing  $\phi$ , whereas  $C_g < 0$  signals an opposite transition. For  $C_g > 0$ , the transitions occur when the branches for both modes merge with the lower boundary of their gap at  $\phi = 0, 2\pi$ , while an opposite occurs when the modes touch the upper boundary of the gap at  $\phi = \pi$ . (See SM [27] for an additional example for a  $p/q = 1/5$  lattice).

The transition of the edge states is employed for a topological pump that exploits the adiabatic variation of  $\phi$  along a second dimension [19]. We illustrate the concept in an array of continuous waveguides (beams) aligned along the  $y$  direction, and coupled by distributed springs of constant  $\gamma_n$  along  $x$  (Fig. 3(a)). The springs react proportionally to the relative transverse displacement (also along  $x$ ) of neighboring beams, so that the governing equation for the  $n$ -th beam reads

$$EI \frac{\partial^4 w_n}{\partial y^4} + \rho A \frac{\partial^2 w_n}{\partial t^2} + (\gamma_{n-1} + \gamma_n) w_n - \gamma_{n-1} w_{n-1} - \gamma_n w_{n+1} = 0, \quad (7)$$

where  $w_n$  is the displacement of the  $n$ -th beam, while  $\rho, E, A$  and  $I$  denote respectively mass density, Young's modulus, cross-sectional area and second moment of area of each beam. Imposing plane wave harmonic motion along  $y$ , *i.e.*  $w_n(y, t) = w_n e^{-i(\omega t - \kappa_y y)}$  where  $\kappa_y$  is the wavenumber, gives

$$(\rho A \omega^2 - EI \kappa_y^4) w_n = (\gamma_n + \gamma_{n-1}) w_n - \gamma_n w_{n+1} - \gamma_{n-1} w_{n-1}. \quad (8)$$

Equation (8) is of the same form as the lattice equation (Eqn. (3)). Thus, similar topological considerations can be made for modulations of the coupling stiffness in the form  $\gamma_n = \gamma_0 \left[ 1 + \alpha \cos \left( 2\pi n \frac{p}{q} + \phi \right) \right]$ . Considering again  $p, q$  as co-primes, *e.g.*  $p/q = 1/3$ , and enforcing Bloch conditions  $w_{n+q} = e^{i\mu_x} w_n$  leads to an eigenvalue problem in the form  $\mathbf{K}(\mu_x, \phi) \mathbf{w} = \lambda^2 \mathbf{w}$ , where  $\mathbf{K}$  is the same stiffness matrix that appears in Eqn. (4). The only differing term is the expression of the eigenvalue  $\lambda^2 = (\Omega^2 - \beta_y^4)$ , where  $\Omega = \omega/\omega_0$ , with  $\omega_0^2 = \rho A/\gamma_0$ , and  $\beta_y = \kappa_y (EI/\gamma_0)^{1/4}$ . For arrays with a finite number  $N$  of beams, letting  $\beta_y = 0$  and  $\phi \in [0, 2\pi]$  produces a diagram identical to that of Fig. 2(b), with edge states spanning the bulk gaps. Variation of  $\beta_y$  shifts the entire spectrum, including the edge states, as shown for a system of  $N = 15$  beams in Fig. 3(b), where frequencies  $\Omega(\phi, \beta_y)$  of the edge states are represented by red surfaces, while the bulk bands are the shaded gray volumes. Motivated by the topological pumping process described next, the dispersion surfaces are displayed in the range  $\phi \in [1.75\pi, 2.25\pi]$ , which corresponds to  $\phi \in [-0.25, 0.25\pi]$  due to the periodicity of  $\gamma_n(\phi)$ . As in 1D lattices, variations of  $\phi$  lead to transitions of the edge states. The dashed and solid red lines at  $\beta_y = 0.8$  in Fig. 3(b) respectively denote left-localized and right-localized modes, and illustrate the transition at  $\phi = 2\pi$  that occurs along the entire surface of the edge states.

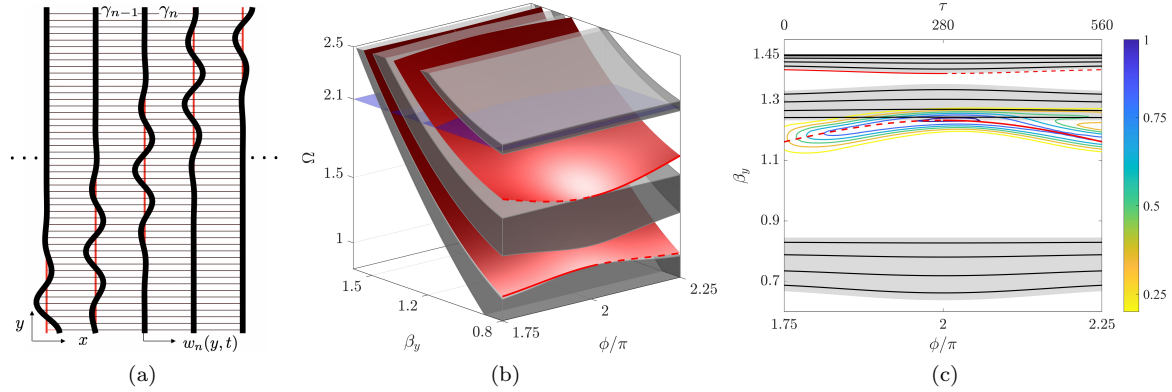


FIG. 3. Dispersion properties for system of coupled beams. (a) Schematic of the lattice of coupled beams: thick black lines show the beams in a notional deformed configuration, while the red lines correspond to the undeformed state. The thin black horizontal lines depict the distributed springs of constant  $\gamma_n$  coupling the beams. (b) Dispersion  $\Omega(\phi, \beta_y)$  for array comprising  $N = 15$  identical beams with stiffness parameters  $p/q = 1/3$ ,  $\alpha = 0.6$ . (c) Wavenumber  $\beta_y$  as function of  $\phi$  for fixed frequency  $\Omega = 2.1$ , corresponding to the cross-section illustrated by the blue plane in (b). The contours represent the Fourier decomposition of the displacement field  $|\hat{W}(\tau, \beta_y)|$ , revealing the adiabatic evolution experienced by the waves.

To implement the pump, we first observe a cross section of the dispersion diagram of Fig. 3(b) at a given frequency (blue plane at  $\Omega = 2.1$  in Fig. 3(b)), which is shown in Fig. 3(c). The bulk bands (shaded gray areas) are populated by the modes of the finite system (solid black lines), while the edge states in the gaps are again highlighted by the red lines (solid and dashed). By exciting the system of beams at this frequency, and applying a slow modulation of  $\phi$  along  $y$ , topological pumping can be induced through the adiabatic [32] evolution of one of the edge states. In contrast to time-modulated materials, the pumping in spatially modulated lattices occurs at a single frequency along the wavenumber branch of the edge state. To demonstrate this, we consider a system of  $N = 15$  coupled beams that are infinite along  $+y$  and are excited at  $y = 0$  by an imposed displacement in the form of a 50-cycle sine burst signal of center frequency  $\Omega = 2.1$ , and  $x$ -wise spatial distribution corresponding to the localized mode in the first gap of Fig. 3(c). The parameter  $\phi$  is varied linearly along  $y$  from  $\phi_1 = 1.75\pi$  to  $\phi_2 = 2.25\pi$  to induce the mode transition from left-localized to right-localized. The response of the lattice is evaluated using the frequency domain formulation of the equations of motion, as detailed in the SM [27], which allows for a solution that is computationally efficient and free from potential inaccuracies caused by spatial polynomial discretization. The simulation results of Fig. 4 show the lattice

deformed configuration at 3 subsequent normalized time instants  $\tau = \omega_0 t$ . The figures illustrate the transition from left-localized wave (left), to a bulk wave (middle), and finally to a right-localized wave (right) that characterizes the pump. The video animation of the full transient response is provided in SM [27].

To illustrate the adiabatic nature of the pump, we perform a time-frequency analysis to represent the displacement field in the reciprocal space  $\hat{W}(\tau, \Omega, \mu_x, \beta_y)$  as a function of time. For visualization purposes, the  $L^2$  norm along the  $\{\Omega, \mu_x\}$  dimensions is then taken so that a function of only time and normalized wavenumber  $\beta_y$  remains, *i.e.*  $\hat{W}(\tau, \beta_y)$ . The results are displayed as contour plots in Fig. 3(c), where the color represents the normalized magnitude of the decomposed displacement field  $|\hat{W}(\tau, \beta_y)|$ . The procedure reveals the evolution experienced by the waves: their amplitude is initially distributed around wavenumbers  $\beta_y$  corresponding to the excited left-localized topological mode, and, as time elapses, it follows the evolution of that mode. At the end of the process, most of the energy is concentrated on the right-localized mode, while some energy is scattered to a neighboring bulk mode. Under the conditions stated by the adiabatic theorem [32], such scattering is expected to occur near the transition point  $\phi = 2\pi$ , where the eigenvalue of the topological mode approach that of the neighboring bulk mode.

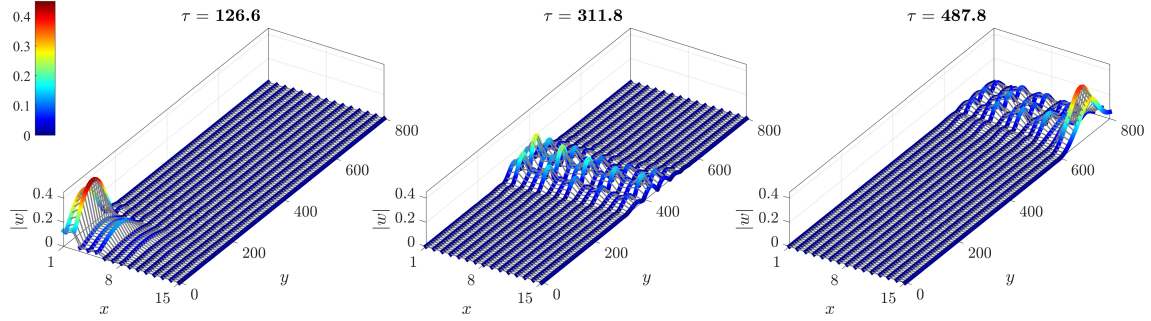


FIG. 4. Topological pumping through adiabatic evolution of the edge state. Snapshots of three time instants illustrate the transition from left-localized, to bulk and finally to right-localized mode as the wave propagates along the  $y$  direction. Deformed configurations show absolute value of beam deflections  $|w_n(y, t)|$ , represented along the vertical direction and also quantified by the associated colormap for ease of visualization.

We investigate the implementation of a topological pump through spatial modulation of the properties of elastic lattices. **The presented results open avenues for the implementation of adiabatic topological pumping in continuous elastic media where material properties and/or geometry can be designed to produce spatial stiffness or inertia modulations. The proposed framework allows the study of systems with properties that are generally modulated along a second dimension, both spatial and temporal. In future work the role of non-linear interactions may be explored in the context of amplitude-dependent behavior [33], robustness of the edge states [34], and as gap opening mechanism in analogy with Mott insulators [35].** The results provide guidelines for future designs of structural components or acoustic waveguides capable of selectively guiding waves along desired paths, and of localizing perturbation in predefined regions of the domains.

The authors acknowledge the support from the National Science Foundation (EFRI 1741685 grant) and of the Brazilian agency FAPESP through project 2016/22432-2.

---

[1] M Zahid Hasan and Charles L Kane. Colloquium: topological insulators. *Reviews of Modern Physics*, 82(4):3045, 2010.

[2] Ling Lu, John D Joannopoulos, and Marin Soljačić. Topological photonics. *Nature Photonics*, 8(11):821, 2014.

[3] Z Yang, F Gao, X Shi, X Lin, Z Gao, Y Chong, and B Zhang. Topological acoustics. *Physical review letters*, 114(11):114301, 2015.

[4] Jiuyang Lu, Chunyin Qiu, Liping Ye, Xiyang Fan,

Manzhu Ke, Fan Zhang, and Zhengyou Liu. Observation of topological valley transport of sound in sonic crystals. *Nature Physics*, 13(4):369, 2017.

[5] SH Mousavi, AB Khanikaev, and Z Wang. Topologically protected elastic waves in phononic metamaterials. *Nature communications*, 6:8682, 2015.

[6] K v Klitzing, Gerhard Dorda, and Michael Pepper. New method for high-accuracy determination of the fine-structure constant based on quantized hall resistance. *Physical Review Letters*, 45(6):494, 1980.

[7] David J Thouless, Mahito Kohmoto, M Peter Nightingale, and Md den Nijs. Quantized hall conductance in a two-dimensional periodic potential. *Physical Review Letters*, 49(6):405, 1982.

[8] P Wang, L Lu, and K Bertoldi. Topological phononic crystals with one-way elastic edge waves. *Physical review letters*, 115(10):104302, 2015.

[9] LM Nash, D Kleckner, A Read, V Vitelli, AM Turner, and WTM Irvine. Topological mechanics of gyroscopic metamaterials. *Proceedings of the National Academy of Sciences*, 112(47):14495–14500, 2015.

[10] A Souslov, BC van Zuijden, D Bartolo, and V Vitelli. Topological sound in active-liquid metamaterials. *Nature Physics*, 13(11):1091, 2017.

[11] NP Mitchell, LM Nash, D Hexner, AM Turner, and WTM Irvine. Amorphous topological insulators constructed from random point sets. *Nature Physics*, page 1, 2018.

[12] R Süsstrunk and SD Huber. Observation of phononic helical edge states in a mechanical topological insulator. *Science*, 349(6243):47–50, 2015.

[13] RK Pal, M Schaeffer, and M Ruzzene. Helical edge states and topological phase transitions in phononic systems using bi-layered lattices. *Journal of Applied Physics*, 119(8):084305, 2016.

[14] M Miniaci, RK Pal, B Morvan, and M Ruzzene. Experimental observation of topologically protected helical edge modes in patterned elastic plates. *Physical Review X*, 8(3):031074, 2018.

- [15] Jiujia Chen, Hongbo Huang, Shaoyong Huo, Zhuhua Tan, Xiaoping Xie, Jianchun Cheng, and Guo-liang Huang. Self-ordering induces multiple topological transitions for in-plane bulk waves in solid phononic crystals. *Physical Review B*, 98(1):014302, 2018.
- [16] Rajesh Chaunsali, Chun-Wei Chen, and Jinkyu Yang. Subwavelength and directional control of flexural waves in zone-folding induced topological plates. *Physical Review B*, 97(5):054307, 2018.
- [17] T Ozawa, HM Price, N Goldman, O Zilberberg, and I Carusotto. Synthetic dimensions in integrated photonics: From optical isolation to four-dimensional quantum hall physics. *Physical Review A*, 93(4):043827, 2016.
- [18] YE Kraus and O Zilberberg. Quasiperiodicity and topology transcend dimensions. *Nature Physics*, 12(7):624–626, 2016.
- [19] YE Kraus, Y Lahini, Z Ringel, M Verbin, and O Zilberberg. Topological states and adiabatic pumping in quasicrystals. *Physical review letters*, 109(10):106402, 2012.
- [20] M Verbin, O Zilberberg, YE Kraus, Y Lahini, and Y Silberberg. Observation of topological phase transitions in photonic quasicrystals. *Physical review letters*, 110(7):076403, 2013.
- [21] Oded Zilberberg, Sheng Huang, Jonathan Guglielmon, Mohan Wang, Kevin P Chen, Yaacov E Kraus, and Mikael C Rechtsman. Photonic topological boundary pumping as a probe of 4d quantum hall physics. *Nature*, 553(7686):59, 2018.
- [22] David J Apigo, Kai Qian, Camelia Prodan, and Emil Prodan. Topological edge modes by smart patterning. *Physical Review Materials*, 2(12):124203, 2018.
- [23] Philip George Harper. Single band motion of conduction electrons in a uniform magnetic field. *Proceedings of the Physical Society. Section A*, 68(10):874, 1955.
- [24] Serge Aubry and Gilles André. Analyticity breaking and anderson localization in incommensurate lattices. *Ann. Israel Phys. Soc*, 3(133):18, 1980.
- [25] VM Alvarez and MD Coutinho-Filho. Edge states in trimer lattices. *arXiv preprint arXiv:1810.05566*, 2018.
- [26] David M Burton. *Elementary number theory*. Tata McGraw-Hill Education, 2006.
- [27] See supplemental material at xxxx for more details, which includes refs. [36, 37], and for a video animation of the transient simulation.
- [28] Y Hatsugai. Chern number and edge states in the integer quantum hall effect. *Physical review letters*, 71(22):3697, 1993.
- [29] Takahiro Fukui, Yasuhiro Hatsugai, and Hiroshi Suzuki. Chern numbers in discretized brillouin zone: efficient method of computing (spin) hall conductances. *Journal of the Physical Society of Japan*, 74(6):1674–1677, 2005.
- [30] Y Hatsugai. Topological aspects of the quantum hall effect. *Journal of Physics: Condensed Matter*, 9(12):2507, 1997.
- [31] Y Hatsugai. Edge states in the integer quantum hall effect and the riemann surface of the bloch function. *Physical Review B*, 48(16):11851, 1993.
- [32] H Nassar, H Chen, AN Norris, and GL Huang. Quantization of band tilting in modulated phononic crystals. *Physical Review B*, 97(1):014305, 2018.
- [33] Raj Kumar Pal, Javier Vila, Michael Leamy, and Massimo Ruzzene. Amplitude-dependent topological edge states in nonlinear phononic lattices. *Physical Review E*, 97(3):032209, 2018.
- [34] Javier Vila, Glaucio H Paulino, and Massimo Ruzzene. Role of nonlinearities in topological protection: Testing magnetically coupled fidget spinners. *Physical Review B*, 99(12):125116, 2019.
- [35] Michael Lohse, Christian Schweizer, Hannah M Price, Oded Zilberberg, and Immanuel Bloch. Exploring 4d quantum hall physics with a 2d topological charge pump. *Nature*, 553(7686):55, 2018.
- [36] James F Doyle. Wave propagation in structures: spectral analysis using fast discrete fourier transforms. *Mechanical Engineering Series*, 1997.
- [37] Jean Bellissard and Barry Simon. Cantor spectrum for the almost mathieu equation. *Journal of functional analysis*, 48(3):408–419, 1982.